

Prospects of designing gold-nanoparticles-based soft terahertz radiation sources and terahertz-to-infrared converters for concealed object detection technology

K. A. Moldosanov^{a)}

Kyrgyz-Russian Slavic University, 44 Kiyevskaya St., Bishkek 720000, Kyrgyzstan

A. V. Postnikov

LCP-A2MC, University of Lorraine, 1 Bd Arago, F-57078 Metz, France

V. M. Lelevkin and N. J. Kairiev

Kyrgyz-Russian Slavic University, 44 Kiyevskaya St., Bishkek 720000, Kyrgyzstan

The two-phonon scheme of generation of terahertz (THz) photons by gold nanobars (GNBs) is considered. It is shown that in GNBs, by choosing their sizes, it is possible to provide conditions for converting the energy of longitudinal phonons with THz frequencies into the energy of THz photons. The prospects of designing GNBs-based soft THz radiation sources (frequencies: 0.14; 0.24; 0.41 and 0.70 THz) with a large flow cross-section (diameter ~ 40 cm) intended for detection of hidden objects under clothing to ensure security in public places (airports, railway stations, stadiums, etc.) are assessed. The choice of the above frequencies is a compromise between the requirements of low absorption of THz radiation by water vapor in air, good penetration through the fabric of clothing, favoring a sufficient resolution of the imaging system, and an abundance of corresponding longitudinal phonons, capable of exciting Fermi electrons in GNBs. Estimates of the characteristics of the terahertz-to-infrared converter based on gold nanospheres (GNSs), which could work in tandem with these sources of THz radiation – as a means of visualization of hidden objects – are also given.

Keywords: gold nanobar, infrared camera, longitudinal phonon, microwave, on body concealed weapon detection, soft terahertz radiation source, terahertz-to-infrared converter

I. INTRODUCTION

From the very beginning of practical exploring the terahertz (THz) range, attempts have been made to apply it for remote detection of hidden threats on the human body – see, e.g., Ref. 1–14 and references therein. Fig. 1 illustrates the geometry of active remote weapon detection (gun, bomb, knife, etc.) hidden under the clothes. In this method of detecting threats on the subject's body, the latter is irradiated by an external source of THz radiation, and radiation reflected from hidden objects is recorded. Previous works allowed to identify the main problems complicating a successful application of THz radiation for the remote detection of hidden objects, namely, an attenuation of THz radiation in fabrics of clothes, and its absorption by water vapor in the air. It was found that the highest transmittance of clothing tissue is in the low-frequency part ($\sim 0.1 - 0.5$ THz) of the THz range. In this range, the attenuation of THz radiation in air water vapor is relatively low, but monotonically increases with increasing frequency and is saturated with damping peaks due to the absorption by oscillating hydrogen atoms in the water molecule. The latter limits the detection range; however, in most hidden object detection systems, the detection range is anyway relatively short, from 1 to 20 m.¹³ As for the application for short-range operation (< 4 m), such as airport security check,

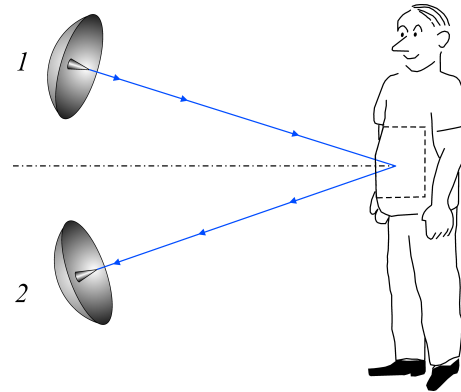


FIG. 1. Typical geometry of the remote threat detection. 1: THz radiation source, 2: THz radiation detector.

the lower operating frequency (~ 0.1 THz) can still provide diffraction-limited image resolution of ~ 2 cm, which should suffice for many threat scenarios.

The development of active methods for detecting hidden objects revealed a shortage of sources of soft THz radiation with a wide radiation flux. Typically, the THz radiation source would be required to create a spot on the human body with a diameter of ~ 40 cm. Accordingly, the imaging system aperture A must be at least this size. As a rule, THz radars with an aperture of $\sim 50 - 100$ cm are used,^{6–11} which is a compromise between the resolution Δx of the imaging system, the range of observation of the subject d and the THz radiation wavelength λ , in

^{a)}Electronic mail: altair1964@yandex.ru

TABLE I. Some numerical parameters for photons at four frequencies selected for our analysis

Frequency ν (THz)	Wavelength (mm)	Photon energy $h\nu$ (meV)	Photon momentum p_{ph} (10^{-26} g cm s $^{-1}$)	Objective resolution* $\Delta x \approx \lambda d/A$ (cm)	Penetration depth † (μm)
0.14	2.1	0.58	3.1	4.2	0.20
0.24	1.25	0.99	5.3	2.5	0.15
0.41	0.73	1.70	9.1	~ 1.5	0.12
0.70	0.43	2.90	15.5	~ 0.9	0.09

*for $d \sim 10$ m, $A \sim 0.5$ m; † skin layer thickness in bulk Au

accordance with the formula for a diffraction-limited resolution: $\Delta x \approx \lambda d/A$. Naturally, the wavelength λ is chosen so that it is not at the same time at the peak of attenuation in the atmospheric air and belongs to the region of acceptable transmission of clothing fabrics, that is, the compromise wavelengths correspond to frequencies $\sim 0.1 - 0.5$ THz. The resolution accessible is within the range $\Delta x \sim 0.5 - 2$ cm.

In the present paper we suggest the novel soft terahertz radiation sources based on gold nanobars (GNBs) being irradiated with microwaves. This approach assesses the feasibility of the idea to convert the energy of longitudinal phonons into electromagnetic energy of THz photons. The approach seems to be reinforced by recent reports^{15–17} on an enhancement beyond the blackbody limit of radiative heat transfer in nanometric-scale objects, as well as by our own estimates of the surface power density of spontaneous THz radiation by gold nanoparticles (see Appendix A).

To enhance the power of THz radiation, GNBs provide the conditions (see Appendix B) to increase the number of longitudinal phonons by heating GNBs with microwave radiation. This approach would enable a wide beam of THz radiation to be issued from a large number of GNBs distributed on a substrate or within a matrix of suffi-

ciently large size.

Taking into account the data of Ref. 11–13 on the attenuation of THz radiation in the air, we have chosen the following frequencies to detect hidden objects: 0.14; 0.24; 0.41 and 0.70 THz (the corresponding wavelengths, energies and momenta of THz photons are given in Table I). These frequencies do not fall into the attenuation peaks of THz radiation in air – see Fig. 2, borrowed from Ref. 13. In addition, at these frequencies the undesirable tissue absorption is sufficiently low, whereas the desired transmission, on the contrary, is high.^{11,18} Table I includes also the objective’s resolution Δx , achievable at chosen frequencies, with the distance to the subject $d \sim 10$ m and the aperture $A \sim 0.5$ m.

The paper is organized as follows. Sec. II explains generation of THz radiation by gold nanobars, Sec. III suggests the practical design of the THz source. In Sec. IV, the parameters of the GNSs-based THz-to-IR converter, which could be used to visualize hidden objects at the security checkpoints, are briefly discussed. The paper is concluded by Sec. V and contains two Appendices, A and B.

II. SUGGESTED DESIGN OF SOFT TERAHERTZ RADIATION SOURCES WITH GOLD NANOBARS AS ACTIVE ELEMENTS

In the proposed approach, in a GNB, the Fermi electron is excited by absorbing a longitudinal phonon, and relaxes by releasing a softer longitudinal phonon. The energy difference is brought away by the electron and emitted as a soft THz photon as the electron scatters at the GNB boundary. The physical picture to be considered is somewhat similar to that discussed earlier in Ref. 19–21, with the only difference that in these works the phonon energy was completely converted into the energy of THz phonon. As emphasized in the works cited, the role of gold nanoobjects is to provide free electrons and longitudinal phonons, their respective energy levels being appreciably discretized due to spatial confinement. The microwave radiation serves as a source of energy for maintaining the “phonon bath” that heats the nanoobjects.

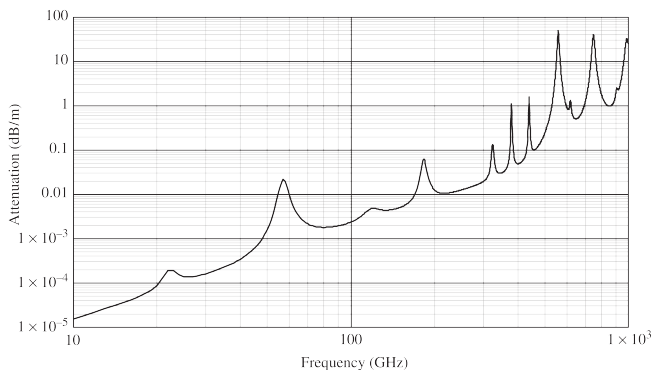


FIG. 2. Electromagnetic waves attenuation by an air layer of 1 m thickness, in the frequency range 0.01 through 1 THz, reproduced from Figure 2.15 of Ref. 13. The frequencies chosen for our analysis are 0.14; 0.24; 0.41 and 0.70 THz.

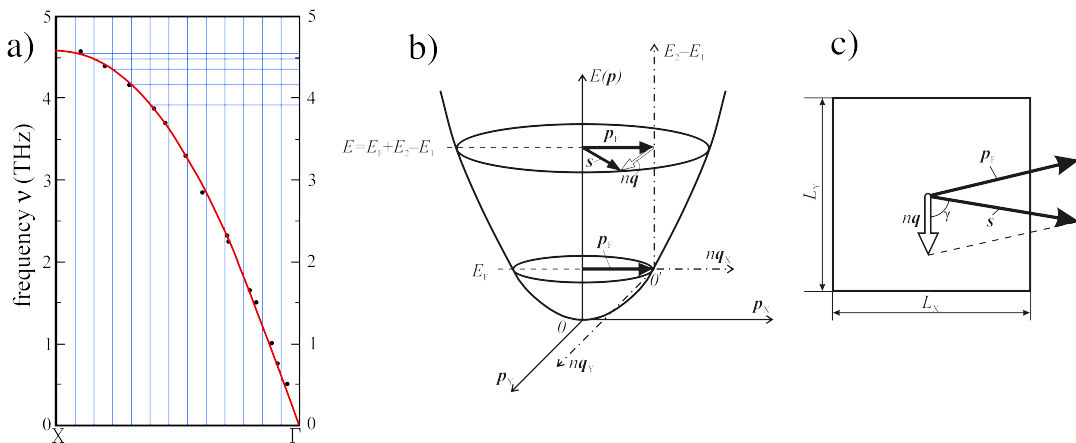


FIG. 3. Energy and momentum relations concerning absorption and subsequent emission of a longitudinal phonon by a Fermi electron. (a) Phonon dispersion in bulk gold along $X - \Gamma$ (red line), discretized as a sequence of spatial confinement (assuming $N_{x,y} = 13$) in a “thin” GNB (vertical blue lines for wavevectors, horizontal blue lines for frequencies). (b) Energy of a Fermi electron as function of (x, y) momenta prior to and after the absorption / emission of longitudinal phonons with energies E_2 / E_1 . \mathbf{p}_F is the Fermi momentum, $n\mathbf{q}$ the difference of phonon momenta, \mathbf{s} the momentum of the electron after the absorption / emission of phonons. (c) The orientation of the three momenta \mathbf{p}_F , $n\mathbf{q}$, \mathbf{s} , making clear the meaning of the angle γ . See text for detail.

A. General considerations

To streamline the argumentation, it seems useful to consider a simplified picture in which the wavevector of the primary (exciting) phonon, \mathbf{q}_2 , and the phonon released in the course of the electron relaxation, \mathbf{q}_1 , are collinear and directed along a short – just several lattice parameters of gold a_{Au} – GNB dimension, say $L_X = N_x a_{\text{Au}}$ or $L_Y = N_y a_{\text{Au}}$ (see Fig. 3), so that the spatial confinement results in discretisation of (x, y) phonon momenta. Now, we assume that the phonon dispersion of bulk gold still approximately holds at the nanoscale (this seems plausible since the vibration spectra of bulk and nanoparticle gold are very close – see Fig. 2 of Ref. 19 and the original papers^{22–24}), and we want to deduce some conclusions from matching the conditions of electron and phonons momenta and energy conservation. Such an analysis has been done in Ref. 25, albeit with compact GNPs (not elongated GNBs) in mind. The discussion around Fig. 2 in Ref. 25 parametrised the experimental $\Gamma - X$ dispersion relation for bulk gold and elaborated on the matching conditions between the energy of absorbed/released phonons, $\hbar\omega(\mathbf{q}_1) - \hbar\omega(\mathbf{q}_2)$, and the quantisation step on the electron excitation.

In the following, these energy / momentum relations are expressed in a more straightforward way, assuming $N_x = N_y = 13$ for the reasons explained in Appendix B. Then $L_X = L_Y = 5.3$ nm, and the momenta of longitudinal phonons are quantized with the step $\hbar/L_X \approx 1.25 \cdot 10^{-20}$ g cm s⁻¹. Fig. 3 summarizes relations between momenta and energies of longitudinal phonons and of Fermi electrons, in the course of absorption / emission of phonons. Fig. 3a depicts the Au dispersion branch along

$X - \Gamma$, divided into \hbar/L_X steps. Different combinations of absorption and emission phonon wavevectors are shown in Table II, along with the corresponding energy differences, expressed also in units of frequency. Of primary interest are the phonons whose frequencies fall into the full width at half maximum (FWHM) of the longitudinal phononic density of modes (shown, e.g., in Fig. 2 of

TABLE II. Energy differences on absorption / emission of longitudinal phonons in gold, consistently with the dispersion relation as shown in Fig. 3. See text for details.

Wavevectors in units of $\frac{(X \rightarrow \Gamma)}{13}$		$E_2 - E_1$ (meV)	ν (THz)	γ
q_2	q_1			
$q_2 - q_1 = 1.25 \times 10^{-20}$ g cm s ⁻¹				
1	2	0.59	0.14	87°
2	3	0.60	0.15	87°
3	4	0.71	0.17	87°
4	5	0.99	0.24	87°
$q_2 - q_1 = 2.50 \times 10^{-20}$ g cm s ⁻¹				
1	3	1.19	0.29	84°
2	4	1.31	0.32	84°
3	5	1.70	0.41	84°
$q_2 - q_1 = 3.75 \times 10^{-20}$ g cm s ⁻¹				
1	4	1.90	0.46	82°
2	5	2.30	0.56	82°
$q_2 - q_1 = 5.00 \times 10^{-20}$ g cm s ⁻¹				
1	5	2.90	0.70	79°

Ref. 19) between ~ 3.9 THz (16.2 meV) and ~ 4.6 THz (19.0 meV), the maximum of the peak in the density of modes being at ≈ 4.2 THz (17.4 meV). The wavevectors of such phonons are close to the Brillouin zone boundary, e.g., separated by just few quantisation steps from the X point. The slope of the frequency/wavevector curve, i.e. the longitudinal speed of sound in this frequency region which will be used in the following to estimate the energy matching conditions, is $v_L^* \approx 1 \cdot 10^5$ cm s $^{-1}$, i.e., considerably reduced in comparison with the nominal (zone-center) speed of sound in bulk gold. The combinations of absorption / emission phonon energies give rise to the energy gain to be transferred to the THz photon (see discussion below); the frequency values appearing in Table II cover the range of “useful” frequencies from 0.14 to 0.70 THz discussed in Section I.

Fig. 3b depicts the electron energy levels of the GNP, indicating explicitly a promotion of the Fermi electron (with momentum \mathbf{p}_F and energy E_F), following an absorption and emission of two phonons with wavevectors close to the Brillouin zone boundary, to an excited state (with momentum \mathbf{s} and energy $E_F + E_2 - E_1$). The relaxation from this excited state will bring about an emission of a THz photon, as argued below. For the moment, we can make two remarks, to elaborate on the electron-phonon part.

The first remark is that the energy of the electron excited state $E_F + E_2 - E_1$ must, in principle, match one of the discrete levels quantized due to confinement within the GNB, in the spirit of the Kubo formula.^{26,27} The step in the “ladder” of electron excitation energies is about $\Delta E_{el} \approx 3.38 \cdot 10^{-3}$ meV, as argued in Appendix B. However, the uncertainty in the phonon energies due to the Heisenberg ratio is about $\delta E_{\text{vibr}} \sim v_L^* \hbar / L_X \approx 0.125$ meV, that makes the above mentioned discreteness of the electron spectrum practically irrelevant, in the context discussed.

The second remark, illustrated by Fig. 3c, is that the electron modifies the direction of its momentum only weakly, and the Fermi momentum of an electron participating at the phonon absorption / emission process is roughly at right angle to the (difference) momentum of the phonons involved. Indeed,

$$\begin{aligned} p_F^2 &= s^2 + (nq)^2 - 2s(nq) \cos \gamma, \quad \text{and} \\ \gamma &= \arccos \frac{s^2 + (nq)^2 - p_F^2}{2s(nq)} \\ &= \arccos \frac{2m(E_2 - E_1) + (nq)^2}{2s(nq)}. \end{aligned} \quad (1)$$

The calculated values of γ for different combinations of absorbed/emitted phonons are given in Table II.

B. Channeling the electron excitation energy into emission of soft THz photons

Following an absorption / emission of “nearly zone-boundary” longitudinal phonons as elaborated above,

one can, in principle, imagine the decay of the excited electron state via promoting an electron across the nanoobject, or via emitting a low-energy phonon, or via a radiative transition. The last process is of interest for us, as it will be the source of soft THz radiation. Here we try to present the argumentation why the two other processes might turn up to be less likely.

The electron mean free path in gold nanoobjects, expectedly shorter than that in nearly perfect bulk crystal, seems to be comparable with the GNB cross-section size; Sec. 9.3.3 of Ref. 28 discusses this issue, in relation to small gold nanoparticles. The situation is therefore likely that the electron will arrive at the GNB surface after none, or very few, scattering events. The electron exit from the GNB is precluded by a prohibitively high value of the work function of gold (4.3 eV²⁹), in comparison with the energy values ($\simeq 1$ meV, see Table II) under discussion. This energy could have been spent onto an emission of a low-energy phonon. The “problem” in this relation is that this ought to be a nearly zone-center phonon, with the nearly linear dispersion characterized by the “nominal” longitudinal speed of sound in gold, $v_L = 3.23 \cdot 10^5$ cm/s.³⁰ However, the slope of $\omega(q)$ near the center of the Brillouin zone is therefore about 3 times more steep than that near the phonon energies of $\simeq 4$ meV, within the FWHM of the peak in the longitudinal density of vibration modes. Due to the quantisation of q depicted in Fig. 3a, the minimal energy “quantum” to excite a low-energy phonon (near Γ) would be $\Delta E_{\text{vibr}} = v_L(\hbar/L_X) \simeq 2.52$ meV. The inspection of $(E_2 - E_1)$ values in Table II shows that such excitation energies do not come about before arriving at combinations with $q_1 = 5$. One can note in this relation that the issue of the Heisenberg’s uncertainty, that was earlier helpful for us to demonstrate that the exact (anyway difficult to control) quantisation of electron energies is of little practical importance, won’t work the same way for phonons: the quantisation step in the vibration energies is $\Delta E_{\text{vibr}} = v_L(\hbar/L_X)$ whereas the Heisenberg’s uncertainty for these energies will be $\delta E_{\text{vibr}} = v_L \delta p_{\text{vibr}} = v_L(\hbar/L_X)$, hence the energy step is always $\sim 2\pi$ times larger than the smearing of each energy separated by this step, whatever the v_L in question.

We note in conclusion that the penetration depth of electromagnetic radiation at the relevant soft THz frequencies (those shown in Table I) exceeds by far the “short” dimensions of the GNBs.

C. Substrate or matrix with gold nanobars for THz source

For nanobars designed to generate soft THz photons, it is important that they are either deposited on a substrate or embedded in a matrix of a material (see Fig. 4) that is not only transparent in the soft THz range, but also withstands sufficiently high temperature heating. Heating nanobars would increase the number of longitudinal phonons in them, which would increase the power of the

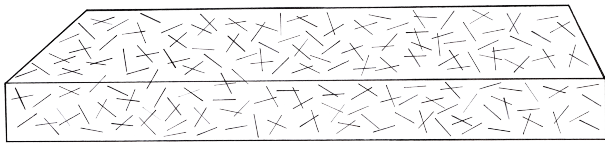


FIG. 4. Soft THz radiation source in the form of a matrix transparent in THz with randomly aligned embedded GNBs.

generated THz radiation. Specifically for the applications in the field of hidden objects detection, the detection range in the THz domain is limited by the absorption by water vapor, therefore increasing the THz source power might be an important issue.

Another way to increase the radiation power is to use a large number of nanobars, deposited on / in a large area of substrate (or matrix); this would also facilitate generating a required large-diameter (~ 40 cm) spot.

Heating nanobars could be carried out by microwave radiation, namely, with the help of a household microwave oven (see Sec. III below); the dimensions of the furnace chamber are large enough to accommodate the substrate / matrix of significant size. In addition, the metal walls of the chamber, reflecting the THz radiation primarily emitted in all directions, would also contribute to a more efficient use of the generated radiation. Conditions for heating the GNBs by microwave radiation see in Appendix B.

Among easily available heat-resistant materials, Teflon[®] is transparent in the THz³¹. The use of a Teflon[®] matrix and application of a standard 2.45 GHz microwave radiation would allow GNBs to be heated to temperatures of about 260 °C. Some matters related to the possible ways of manufacturing the Teflon[®] matrix were considered in our work.³² An even greater increase in the temperature of nanobars could be achieved by using for the substrate or matrix such materials as the high-resistivity float-zone silicon, crystal quartz, or sapphire.³¹

III. POSSIBLE DESIGN OF THE GOLD-NANOBARS-BASED SOFT THz RADIATION SOURCE

The soft THz radiation source could be designed as shown in Fig. 5 (see also patents Ref. 20,21). The housing 1 with metal chamber 2 inside comprises a substrate 3 with GNBs 4 deposited on it (otherwise, a matrix can be used with embedded GNBs). An electromagnetic emitter in the form of a magnetron 5 with a waveguide 6 opens into the chamber; the power, control and cooling systems are not shown. In the housing 1, an opening 8 is made, in which a resonant filter 7 for the outgoing THz radiation is installed. Beyond the filter 7, a focusing system 9 can be placed, collecting the THz radiation emitted by GNBs 4 and focusing it on a hidden object 10 on the subject under examination. Filters and lenses for the

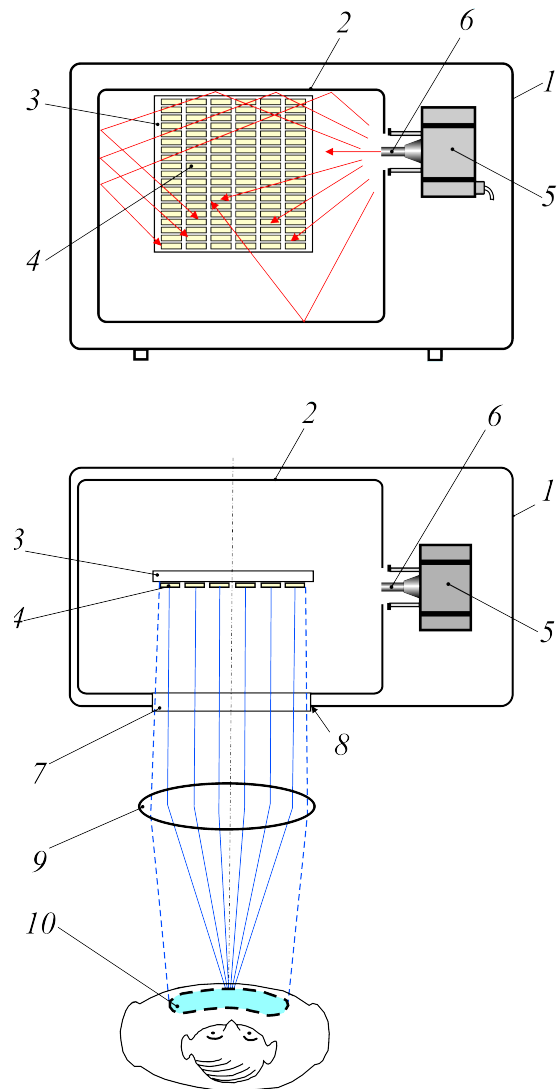


FIG. 5. Possible construction of the GNBs-based soft THz radiation source. Upper panel: front view, lower panel: top view. See text for discussion.

THz range are commercially available and manufactured, for example, by the TYDEX[®].^{33,34}

The source operates as follows. The magnetron generates microwave photons, which enter the cavity and heat the GNBs, that is manifested as an increase in the number of longitudinal phonons.

As was argued above, those Fermi electrons in the GNBs which undergo an absorption / emission of phonons along the scenario elaborated in Sec. II end up in an excited state the relaxation from which can not proceed by exiting the sample (the work function of gold being prohibitively high) nor via emission of a low-energy (close to the zone center) phonon.

When using a THz radiation source to scan humans, that is, for a non-covert examination at short distances (≤ 1 m) to detect objects hidden under clothing, the fo-

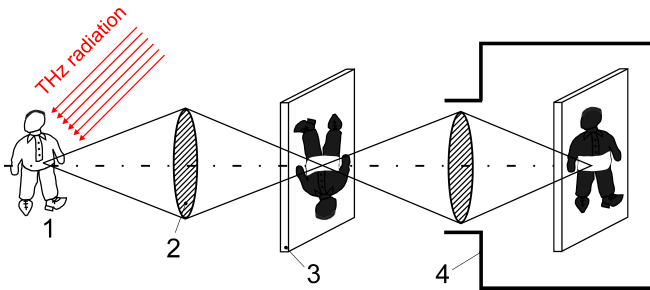


FIG. 6. Detection and imaging of objects concealed under clothing. 1: the person inspected; 2: objective focusing the reflected THz radiation onto the converter; 3: THz-to-IR converter; 4: IR camera.

cusing system 9 might be left out. In this case, instead, an unfocused flow of THz radiation is required, which would provide a spot with a diameter of ~ 40 cm on the human body. THz photons reflected from the metal parts of the hidden object are recorded by the THz detector (see Figs. 1 and 6). As a possible realization of the latter, a THz-to-IR converter could be used, similar to that suggested for visualization of malignant tumour.³⁵ More detailed estimations of the expected parameters of this device’s performance can be found in Ref. 32.

IV. THz TO IR CONVERTER FOR VISUALIZATION OF HIDDEN OBJECTS

The second essential component of the proposed concealed object detection system is the setup for visualization of scattered / reflected THz image; the idea is to convert the distribution of intensities over the THz wavefront into the map of temperatures, and inspect the latter with the help of a standard IR camera. The working element of the THz to IR converter is the plate covered with a sufficiently dense array of gold nanospheres (GNS), to be heated under the effect of incoming THz radiation, or the matrix bearing such objects densely embedded within.

Fig. 6 outlines the general suggested scheme of the detection setup. The subject 1 is irradiated with a soft THz radiation source. The radiation reflected from the object hidden on the subject’s body is focused by the lens 2 on the THz-to-IR converter 3 and creates the hidden object’s image in THz rays on the converter plate. The converter absorbs THz radiation and channels its energy into excitation of longitudinal phonons, that amounts to local heating and creation of a point source of IR radiation associated with each single gold nanosphere (GNS). The resulting two-dimensional picture of IR “pixels” is perceived by a standard IR camera 4 and made visible on the camera’s display. Technical considerations to be elaborated include (i) the choice of acceptable GNS sizes to ensure a good “performance” of a single GNS as heat emitter, in view of reaction time and the spatial dissipa-

tion of heat into the substrate or matrix, that will blur the “pixel”, and (ii) the distribution of GNSs within the converter’s plate to ensure sufficient sensitivity and spatial resolution of thermal picture to be perceived by the IR camera.

If the matrix’ thickness δ is within the depth of focus l_{dof} of the IR camera’s objective, the matrix seems preferable over single-layer deposition, because it allows to achieve larger “projected” density of GNSs per surface unit. In the following analysis, we assumed $\delta = 0.1$ mm (of the Teflon[®] film) and $l_{\text{dof}} \approx 0.3$ mm, therefore, we have done all estimations for the matrix (Fig. 7).

Table III outlines the parameters of GNSs to be embedded into the Teflon[®] matrix so that to yield the converter’s reasonable efficiency. The basic considerations, including estimations of the GNSs diameters, are evoked and discussed in Ref. 32. In a nutshell, on absorbing a THz photon by a GNS, the (presumed nearly free) Fermi electron is excited across m_{el} steps of (confinement-imposed) energy ladder, and then relaxed by releasing a longitudinal phonon with n_{vibr} minimal steps in wavevector and/or energy, assuming the linear dispersion for phonons. The mismatch in the momentum conservation on such process, that would normally come about due to different dispersion relations for photons, electrons and phonons, will be tolerated by force of the Heisenberg’s uncertainty relation, as argued in Ref. 32. Specifically, the confinement-conditioned uncertainty of the electron momentum in a particle of diameter D , $\Delta p_D \approx h/(2\pi D)$, should exceed Δp_F , the mismatch of momentum of the Fermi electron on absorption of the THz photon of frequency ν . The corresponding estimates are listed in Table III for four target frequencies specified in Sec. I. For all these frequencies, the soft THz radiation easily penetrates the particle (cf. “skin depth” values in Table I), so that all Fermi electrons can participate in the absorption of THz photons.

The upper part of the Table III deals with isolated GNSs; the lower part concerns the latter’s embedding in Teflon[®], as a likely candidate for the substrate material. The data on the 0.1 mm thick Teflon[®] film transmissions are from Ref. 31. The emissivity factor α , a phenomenological property of “real” nanoparticles, indicates which part of the energy delivered will then emerge via IR radiation; the values $\alpha=1$ to 0.5 will presumably bracket the realistic estimates. ΔT_α is the excess of temperature over the background to be created in the GNS to make

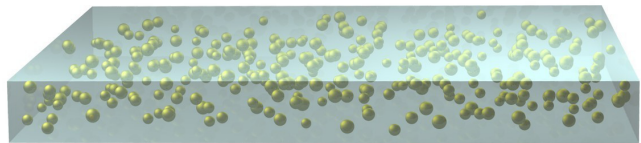


FIG. 7. THz-to-IR converter in the form of the matrix with embedded GNSs.

TABLE III. Parameters of GNSs intended for registration of soft THz radiations, for the pixel size $d = 15 \mu\text{m}$ and the thickness of the Teflon[®] matrix $\delta = 0.1 \text{ mm}$. Concentration of GNSs in the matrix is $(d^2 \delta)^{-1} = 4.44 \cdot 10^4 \text{ mm}^{-3}$.

Property	Units	Frequency (THz)							
		0.14		0.24		0.41		0.70	
Phonon momentum	h/a_{Au}	0.020		0.024		0.050		0.090	
Phonon momentum	10^{-21} g cm/s	3.25		5.35		8.11		14.60	
m_{el}		36		12		5		2	
n_{vibr}		1		1		1		1	
$D \approx 4.23(m_{\text{el}}/n_{\text{vibr}})^{1/2}$	nm	25.4		14.65		9.5		6.0	
Thermal conductivity λ_{1p}	$\text{W m}^{-1}\text{K}^{-1}$	220.1		126.9		82.3		52.0	
Δp_D	10^{-21} g cm/s	≥ 0.41		≥ 0.72		≥ 1.11		≥ 1.76	
Δp_F	10^{-23} g cm/s	0.66		1.135		1.94		3.31	
Transmission of the 0.1 mm thick Teflon [®] film	%	~ 90		~ 90		~ 92		~ 92	
Emissivity factor α		1	0.5	1	0.5	1	0.5	1	0.5
ΔT_α	mK	14	28	14	28	14	28	14	28
Q_T	10^{-10} W	5.96	11.91	3.40	6.79	2.19	4.38	1.38	2.75
Threshold number of GNSs within volume element ($d^2 \delta$) that maps onto a pixel of IR camera		0.08		0.13		0.21		0.33	
Heating time	μs	0.57	0.56	0.43	0.43	0.33	0.33	0.23	0.23
Cooling time	μs	1.53	1.58	1.32	1.39	1.38	1.36	1.18	1.19
Radius at which the temperature in the Teflon [®] matrix falls to 1/10 that in the GNS centre	nm	100.0		62.3		42.0		27.3	
Operating power of the $9.6 \times 7.7 \times 0.1 \text{ mm}^3$ Teflon [®] matrix with embedded GNSs of diameter D	μW	195.6	390.9	111.6	222.9	71.9	143.8	45.3	90.3

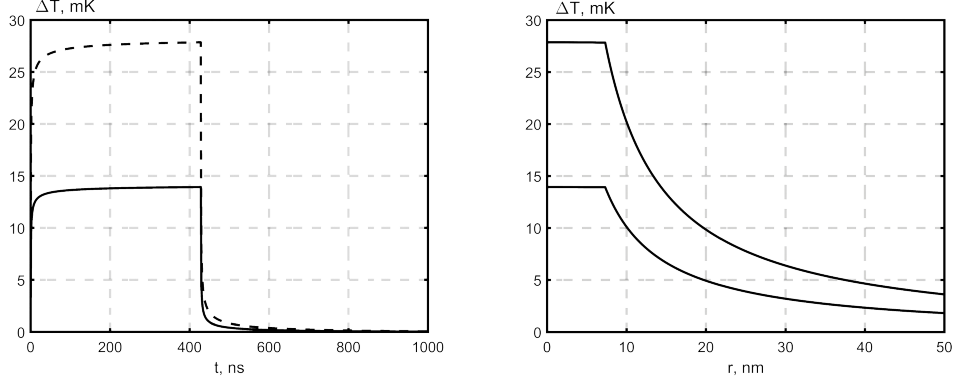


FIG. 8. Time characteristics (left panel) and radial temperature distributions (right panel) around the GNS with a diameter of 14.65 nm (for visualization at 0.24 THz) in the Teflon[®] film matrix for two values of the emissivity factor, $\alpha=1$ (lower curve) and $\alpha=0.5$ (upper curve).

it detectable by the IR camera; the nominal sensitivity value of $\approx 14 \text{ mK}$, characterizing modern IR cameras, needs to be increased in case of reduced values of α . In order to attain such temperature on the GNS, the power Q_T needs to be delivered, which follows from the solution of the heat transfer equation. With Q_T as a source term, the heat equation describes the rise of temperature with time and the radial temperature profile across

the GNS and its surrounding medium. These properties are depicted in Fig. 8 for the particle with diameter $D = 14.65 \text{ nm}$ embedded in Teflon[®].

From Fig. 8 (left panel) and from Table III one can conclude that THz-to-IR converter built along the concept outlined should possess the heating / cooling times acceptable for real-time operation, and operating power in the range of accessible.³⁶⁻³⁹ Thus, the THz sources

discussed, as well as the visualization system based on the THz-to-IR converter, could find application in the equipment for detection of hidden objects.

Note that some issues related to improving the efficiency of conversion of THz radiation into heat by nanoobjects were discussed in our article,²⁵ and issues related to possible methods of manufacturing a matrix from Teflon[®] were considered in Ref. 32. Since the matrix with embedded GNSs is not commercially available, we mention a method that may be useful in the laboratory conditions. For the matrix, one could take gelatin, a water soluble protein transparent in the soft THz range. For embedding into the matrix, one may find it convenient to use commercial GNSs which are sold in the form of water suspensions.

The data on the transparency of the pure gelatin in the THz range are scarce, therefore for the estimates one could use the graph of the transmission spectrum of the silver-ion-doped gelatin matrix spanning a wavelength range of 0.2 μm to 1.5 mm from Ref. 40. Figure 4 in that article shows that there is a transmission window in the THz range, which notably spans the wavelengths corresponding to “our” chosen soft THz frequencies (see Table I). The transmission of gelatin is relatively high ($\sim 80\%$) at 1.25 mm wavelength, but drops down to $\sim 50\%$ at 0.43 mm. Although at wavelengths larger than 1 mm the transmission seems to be gradually declining, one can extrapolate the trend to an acceptable value of $\sim 75\%$ at the 2.1 mm wavelength.

V. CONCLUSION

Summarizing, we outlined a concept of soft THz radiation sources in the form of the matrix (high-resistivity float-zone silicon, crystal quartz, sapphire or Teflon[®]), into which the gold nanobars are embedded. A specificity of soft THz radiation, for which we selected for our analysis the photons with frequencies of 0.14, 0.24, 0.41 and 0.70 THz is that it may come about in the course of two-phonon processes: first, an excitation of the Fermi electrons with the absorption of the longitudinal phonon, and then the release of a softer longitudinal phonon, whereby the excited electron retains the difference in the energies of the two phonons – respectively, 0.58; 0.99; 1.70 and 2.90 meV for the above frequencies. The relaxation of electrons possessing these excess energy over the Fermi level occurs via emission of THz photons. To increase the number of longitudinal phonons (and, as a result, to increase the emitted THz power), nanoobjects are suggested to be heated with microwave radiation at a standard (domestic micro oven) frequency of 2.45 GHz. To generate THz photons with the frequencies indicated, the gold nanobars with dimensions 5.3 nm \times 5.3 nm \times 1.318 μm seem suitable. Such THz radiation sources being used together with the THz-to-IR converter could be, among other possible applications, be used in the equipment for discovering and visualization

of concealed goods.

Appendix A: Enhanced surface power density of spontaneous THz radiation by gold nanoparticles due to confinement

Here we would like to show just a principal possibility of the significant excess of the Planck limit in the THz range in gold nanoparticles. Namely, the mechanism of photon emission discussed in Sec. II may be characterized by quite elevated surface power density of spontaneous THz radiation. We estimate this effect only by order of magnitude and within a very simplified model: we assume the nanoparticle to be a sphere with diameter $D = 5.3$ nm; further on, we suppose that the release of a secondary phonon occurs simultaneously with the emission of a THz photon by the excited electron.

The D value chosen lets us refer to Fig. 3 and to the discussion related to quantization of states due to confinement on this linear size, without entering the details depending on the exact nanoobject’s shape. For numerical estimations, we limit ourselves by the case of 0.24 THz emitted photons. We estimate the excess, due to spatial confinement, of the radiation emitted over the predictions of the Planck’s law for the black body radiation for two special cases, taking into account the uncertainty in the energy of both the longitudinal phonons and the Fermi electrons.

The uncertainty in the energy of longitudinal phonons

The spatial confinement at the length scale D brings about the uncertainty of the phonon momentum Δp , $\Delta p \cdot D \geq \hbar$. By relation of p to the phonon energy via the (longitudinal) speed of sound v_L^* within the “range of interest” (throughout the FWHM centered at ~ 4 meV, in our case), the uncertainty of energy is

$$\Delta E \approx v_L^* \cdot \Delta p \geq \frac{v_L^* \hbar}{2\pi D}. \quad (\text{A1})$$

For the Fermi electron which absorbed energy ($E_2 - E_1$), the excited state will have an uncertainty $\sim \pm(\Delta E/2)$ around the energy ($E_F + E_2 - E_1$). This would amount to this state being characterized by a finite lifetime Δt such that

$$\Delta E \cdot \Delta t \geq \frac{\hbar}{2\pi}. \quad (\text{A2})$$

Combining the previous relations, the order-of-magnitude estimate of the characteristic lifetime of the excited electron is

$$\Delta t \simeq \frac{\hbar}{2\pi \Delta E} \simeq \frac{D}{v_L^*}, \quad (\text{A3})$$

that gives a physically meaningful estimate of the “flight time” of a phonon across the nanoparticle. The average

emitted THz power can be roughly related to the photon energy $E_2 - E_1 \pm (\Delta E/2)$ released during Δt :

$$\begin{aligned} \langle P_{\text{THz}} \rangle &= \frac{E_2 - E_1 \pm (\Delta E/2)}{\Delta t} \\ &\simeq \left[E_2 - E_1 \pm \frac{v_L^* h}{4\pi D} \right] \frac{v_L^*}{D}. \end{aligned} \quad (\text{A4})$$

In the phononic energy range of FWHM, the speed of sound is $v_L^* \simeq 10^5$ cm/s. The ‘‘energy uncertainty’’ term $\pm (v_L^* h)/(4\pi D) \approx 1 \cdot 10^{-2}$ meV can be neglected compared to $E_2 - E_1 = 0.99$ meV. The emitted power is then $\langle P_{\text{THz}} \rangle \simeq 3 \cdot 10^{-11}$ W, and the surface density of the THz power emitted by the gold nanosphere with the diameter $D = 5.3$ nm:

$$\frac{\langle P_{\text{THz}} \rangle}{4\pi(D/2)^2} \approx 3.4 \cdot 10^5 \text{ W/m}^2. \quad (\text{A5})$$

In order to make comparison with the prediction by the Planck’s theory, we integrate the function

$$\epsilon(\lambda) = \frac{2\pi c^2}{\lambda^5} \frac{h}{\exp\left(\frac{hc}{k\lambda T}\right) - 1}$$

over wavelengths throughout the FWHM, i.e., between $\lambda_{\min} = 6.53 \cdot 10^{-5}$ m and $\lambda_{\max} = 7.76 \cdot 10^{-5}$ m, that yields 2.68 W/m^2 (c is the speed of light in vacuum, h the Planck constant, k the Boltzmann constant, T the temperature assumed to be 300 K).

Note that the estimate Eq. (A5) was performed for a single pair of phonons (with an energy difference of 0.99 meV) within the FWHM. This turned out already sufficient to demonstrate that the Planck formula gravely underestimates in the THz range on a nanometric scale, as was already noted in the works^{15–17} devoted to the study of far-field thermal radiation transfer in nanoscale objects with a size smaller than the Wien’s wavelength λ_W ($\approx 10 \mu\text{m}$ at $T = 300$ K). Experimental studies have shown that deviations from the predictions of the Planck’s theory can reach two to seven orders of magnitude.

Accounting for uncertainty in the energy of the Fermi electrons

Since the Fermi electron velocity in gold $v_F = 1.4 \cdot 10^8$ cm/s is three orders of magnitude higher than the speed of sound in the phononic energy range of FWHM, $v_L^* \simeq 10^5$ cm/s, a similar argumentation hints for an excess over the prediction by the Planck’s formula by three more orders of magnitude, yielding, for gold nanosphere with $D = 5.3$ nm as above, $\langle P_{\text{THz}} \rangle/[4\pi(D/2)^2] \simeq 2.7 \cdot 10^9 \text{ W/m}^2$. (For comparison: the surface density of power radiated by the Sun’s surface is $\simeq 7 \cdot 10^7 \text{ W/m}^2$). Overcoming the Planck limit of the surface power density of radiation inspires attempts to generate soft THz radiation using a large number of

nanoparticles. So it would be possible to make a radiation source of sufficiently large total power, unattainable or difficult to achieve by other ways. By the order of estimate, the total power of the distributed source radiating into the solid angle 4π at frequency 0.24 THz, with a matrix diameter of 200 nm, a thickness of 1 nm, with a concentration of 10^5 mm^{-3} nanoparticles might be $\simeq 94$ mW.

Appendix B: Choice of optimal size for gold nanobars

We discuss now the condition for a microwave photon with energy $h\nu$ (assuming $\nu = 2.45$ GHz, the standard microwave frequency of a domestic oven) to be most efficiently absorbed by a gold nano-object with dimensions $L_X = N_x a_{\text{Au}}$, $L_Y = N_y a_{\text{Au}}$, $L_Z = N_z a_{\text{Au}}$. The absorption excites a Fermi electron into a state with the energy $E_F + m_{\text{el}} \Delta E_{\text{el}}$, several (m_{el}) confinement-dependent quantization steps, $\Delta E_{\text{el}} = \frac{4}{3} E_F/N$ by force of the Kubo formula,^{26,27} above the Fermi energy E_F ($N = 4N_x N_y N_z$ is the number of univalent gold atoms in the nanoparticle). Following the excitation, the electron relaxes on releasing a longitudinal phonon, whereby the nanoparticle is heated. The vibration states are quantized, the smallest step in the momenta values being that in the direction in which the GNB is the longest, i.e., L_Z . The corresponding step in energy, assuming linear dispersion law with the longitudinal speed of sound v_L defining the slope, will be $\Delta E_{\text{vibr}} = v_L h/L_Z$. The conservation of energy imposes

$$h\nu = m_{\text{el}} \Delta E_{\text{el}} = n_{\text{vibr}} \Delta E_{\text{vibr}}. \quad (\text{B1})$$

for some m_{el} and n_{vibr} integer. The conservation of momentum cannot be exactly respected, because the dispersion relations for photons and phonons are markedly different (see Fig. 9.2 and related discussion in Ref. 28). However, the mismatch of momentum can be ‘‘absorbed’’ in the uncertainty of the phonon momentum, $\Delta p \simeq \hbar/L_Z$, which comes about as a (yet another) consequence of spatial confinement. The condition for Δp to help match the momenta will read $\Delta p \geq \Delta p_F$, whence the condition on L_Z (formulated for $\nu = 2.45$ GHz):

$$L_Z \leq \frac{v_F}{2\pi\nu} \approx 91 \mu\text{m}. \quad (\text{B2})$$

Making use of Eq. (B1) formulated in terms of N_x , N_y , N_z , we get

$$m_{\text{el}} = \frac{3h\nu}{E_F} N_x N_y N_z, \quad n_{\text{vibr}} = \frac{\nu a_{\text{Au}}}{v_L} N_z \quad (\text{B3})$$

and hence

$$\frac{m_{\text{el}}}{n_{\text{vibr}}} = \frac{3h v_L N_x N_y}{a_{\text{Au}} E_F}. \quad (\text{B4})$$

We are interested in the small size of the GNBs, because heating a small GNB requires less microwave power. This

implies the smallness of the numbers N_x , N_y , N_z as well as of m_{el} and n_{vibr} . Assuming for simplicity $N_x = N_y$ and applying the numerical values of h , $v_L = 3.23 \cdot 10^5$ cm/s,³⁰ $a_{\text{Au}} = 0.408$ nm²⁹, $E_F = 5.53$ eV,²⁹ we obtain:

$$\frac{m_{\text{el}}}{n_{\text{vibr}}} = 1.777 \cdot 10^{-2} \cdot N_x^2. \quad (\text{B5})$$

We select the minimum value of the n_{vibr} parameter, namely =1, and search for its compatible small enough integer values of m_{el} . It turns out that at $N_x = 13$, $m_{\text{el}} = 3.003 \approx 3$, and for $N_x=15$, $m_{\text{el}} = 3.998 \approx 4$. We retain the smallest value $N_x=13$ for calculations in the present work; in particular, we split the $\Gamma - X$ interval in Fig. 3a into 13 intervals. The GNB's width and height are $L_X=L_Y=N_x a_{\text{Au}}=N_y a_{\text{Au}}=13 \times 0.408$ nm = 5.3 nm. From the relations $n_{\text{vibr}} \cdot \Delta E_{\text{vibr}} = \hbar \nu$ and $\Delta E_{\text{vibr}} = v_L (h/L_z)$, we obtain for the length of GNB: $L_z = n_{\text{vibr}} v_L / \nu$, which for the frequency $\nu=2.45$ GHz yields $L_z=1.318$ μm ($N_z \approx 3230$), whereby $\Delta E_{\text{el}} \approx 3.38 \cdot 10^{-3}$ meV.

The synthesis of single-crystal gold nanowires with lengths of up to several microns has already been mastered.^{41–44} Manufacturing the GNBs of 1.318 μm length will hopefully not be a problem. According to the theoretical analysis,⁴⁵ for gold nanowire to be “stable”, its diameter must be greater than $4.5 a_{\text{Au}}$, i.e., larger than 1.84 nm. Our estimates of the minimal “thickness” of the GNBs well respects this condition.

REFERENCES

- ¹Bjarnason, J. E., Chan, T. L. J., Lee, A. W. M., Celis, M. A., and Brown, E. R., “Millimeter-wave, terahertz, and mid-infrared transmission through common clothing,” *Applied Physics Letters* **85**(4), 519 (2004).
- ²Tribe, W. R., Newnham, D. A., Taday, P. F., and Kemp, M. C., “Hidden object detection: security applications of terahertz technology,” *Proceedings of SPIE* **5354** (Apr 2004). Terahertz and Gigahertz Electronics and Photonics III.
- ³Gatesman, A. J., Danylov, A., Goyette, T. M., Dickinson, J. C., Giles, R. H., Goodhue, W., Waldman, J., Nixon, W. E., and Hoen, W., “Terahertz behavior of optical components and common materials,” *Proceedings of SPIE* **6212**, 62120E (May 2006). Terahertz for Military and Security Applications IV.
- ⁴Kemp, M. C., “Millimetre wave and terahertz technology for the detection of concealed threats: a review,” *Proceedings of SPIE* **6402**, 64020D (Sep 2006). Optics and Photonics for Counterterrorism and Crime Fighting II.
- ⁵Appleby, R. and Wallace, H. B., “Standoff detection of weapons and contraband in the 100 GHz to 1 THz region,” *IEEE Transactions on Antennas and Propagation* **55**, 2944 (Nov 2007).
- ⁶Sheen, D. M., McMakin, D. L., Barber, J., Hall, T. E., and Severtsen, R. H., “Active imaging at 350 GHz for security applications,” *Proceedings of SPIE* **6948**, 69480M (Apr 2008). Passive Millimeter-Wave Imaging Technology XI.
- ⁷Sheen, D. M., McMakin, D. L., Hall, T. E., and Severtsen, R. H., “Active millimeter-wave standoff and portal imaging techniques for personnel screening,” in [2009 *IEEE Conference on Technologies for Homeland Security*], 440 (May 2009).
- ⁸Moeller, L., “Standoff detection of concealed weapons using a terahertz illuminator with an uncooled imager,” tech. rep., Bell Laboratories (Aug 2011).
- ⁹Robertson, D. A., Macfarlane, D. G., Cassidy, S. L., Bryllert, T., Gandini, E., and Llombart, N., “Submillimetre wave 3D imaging radar for security applications,” in [*IET Colloquium on Millimetre-Wave and Terahertz Engineering Technology 2016*], 1 (Mar 2016).
- ¹⁰Cooper, K. B., Dengler, R. J., Llombart, N., Talukder, A., Panagandan, A. V., Peay, C. S., Mehdi, I., and Siegel, P. H., “Fast high-resolution terahertz radar imaging at 25 meters,” *Proceedings of SPIE* **7671**, 76710Y (Apr 2010). Terahertz Physics, Devices, and Systems IV: Advanced Applications in Industry and Defense.
- ¹¹Kemp, M. C., “Explosives detection by terahertz spectroscopy – a bridge too far?,” *IEEE Transactions on Terahertz Science and Technology* **1**, 282 (Sep 2011).
- ¹²Linden, K. J., Neal, W. R., Waldman, J., Gatesman, A. J., and Danylov, A., “Terahertz laser based standoff imaging system,” in [34th *Applied Imagery and Pattern Recognition Workshop (AIPR'05)*], 8 (Oct 2005).
- ¹³Daniels, D. J., [EM *Detection of Concealed Targets*], John Wiley & Sons, Inc. (Dec 2009).
- ¹⁴Li, C. and Fang, G., “Terahertz imaging for security – algorithm and system realization,” *Terahertz Science and Technology* **9**, 19 (Mar 2016).
- ¹⁵Thompson, D., Zhu, L., Mittapally, R., Sadat, S., Xing, Z., McArdle, P., Qazilbash, M. M., Reddy, P., and Meyhofer, E., “Hundred-fold enhancement in far-field radiative heat transfer over the blackbody limit,” *Nature* **561**, 216 (Sep 2018).
- ¹⁶Thompson, D., Zhu, L., Mittapally, R., Sadat, S., Xing, Z., McArdle, P., Qazilbash, M. M., Reddy, P., and Meyhofer, E., “Author correction: Hundred-fold enhancement in far-field radiative heat transfer over the blackbody limit,” *Nature* **567**, E12 (Mar 2019).
- ¹⁷Fernández-Hurtado, V., Fernández-Domínguez, A. I., Feist, J., García-Vidal, F. J., and Cuevas, J. C., “Exploring the limits of super-Planckian far-field radiative heat transfer using 2D materials,” *ACS Photonics* **5**, 3082 (Aug 2018).
- ¹⁸Moldosanov, K. A., Lelevkin, V. M., Kozlov, P. V., and Kaveev, A. K., “Terahertz-to-infrared converter based on metal nanoparticles: potentialities of applications,” *Journal of Nanophotonics* **6**, 061716 (2012).
- ¹⁹Moldosanov, K. and Postnikov, A., “A terahertz-vibration to terahertz-radiation converter based on gold nanoobjects: a feasibility study,” *Beilstein Journal of Nanotechnology* **7**, 983 (2016).
- ²⁰Moldosanov, K. A. and Postnikov, A., “Source of terahertz radiation. Russian patent RU 2622093. Priority: 13.05.2016, date of publication: 09.06.2017 (Bull. 16), corrected: 25.07.2017 (Bull. 21).” <https://patents.google.com/patent/RU2622093C1/en> (2016). Accessed : 14 August 2019.
- ²¹Moldosanov, K. A. and Postnikov, A. V., “Converter of terahertz vibrations into terahertz electromagnetic radiation. Russian patent RU 2650343. Priority: 20.03.2017, date of publication: 11.04.2018 (Bull. 11).” <https://patents.google.com/patent/RU2650343C1/en> (2017). Accessed : 14 August 2019.
- ²²Lynn, J. W., Smith, H. G., and Nicklow, R. M., “Lattice dynamics of gold,” *Phys. Rev. B* **8**, 3493 (Oct 1973).
- ²³Muñoz, J. A., Lucas, M. S., Mauger, L., Halevy, I., Horwath, J., Semiatin, S. L., Xiao, Y., Chow, P., Stone, M. B., Abernathy, D. L., and Fultz, B., “Electronic structure and vibrational entropies of fcc Au-Fe alloys,” *Phys. Rev. B: Condens. Matter* **87**, 014301 (Jan 2013).
- ²⁴Bayle, M., Combe, N., Sangeetha, N. M., Viau, G., and Carles, R., “Vibrational and electronic excitations in gold nanocrystals,” *Nanoscale* **6**, 9157 (2014).
- ²⁵Postnikov, A. V. and Moldosanov, K. A., “Suggested design of gold-nanoobjects-based terahertz radiation source for biomedical research,” *Nanotechnology* **29**, 285704 (Jul 2018).
- ²⁶Kubo, R., “Electronic properties of metallic fine particles. I.,” *J. Phys. Soc. Jpn.* **17**(6), 975 (1962).
- ²⁷Kubo, R., “Discreteness of energy levels in small metallic particles,” *J. Phys. Colloques* **38**, C2–69 (Jul 1977).

- ²⁸Postnikov, A. and Moldosanov, K., “Phonon-assisted radiofrequency absorption by gold nanoparticles resulting in hyperthermia,” in [*Fundamental and Applied Nano-Electromagnetics*], Maffucci, A. and Maksimenko, S. A., eds., *The NATO Science for Peace and Security Programme, Series B: Physics and Biophysics*, 171 – 201, Springer, Dordrecht, The Netherlands (2016). Proceedings of the NATO Advanced Research Workshop on Fundamental and Applied Electromagnetics, Minsk, Belarus, 25-27 May, 2015.
- ²⁹Ashcroft, N. W. and Mermin, N. D., [*Solid State Physics*], Saunders College (1976).
- ³⁰Singh, R. N. and Ali, I., “Elastic moduli and phonon dispersion curves for amorphous metals and alloys,” *International Journal of Applied Physics and Mathematics* **3**, 275 (Jul 2013).
- ³¹“TYDEX[®] THz materials.” http://www.tydexoptics.com/products/thz_optics/thz_materials/. Accessed: 14 August 2019.
- ³²Postnikov, A. V., Moldosanov, K. A., Kairyev, N. J., and Lelevkin, V. M., “Prospects for terahertz imaging the human skin cancer with the help of gold-nanoparticles-based terahertz-to-infrared converter,” in [*Fundamental and Applied Nano-Electromagnetics II*], Maffucci, A. and Maksimenko, S. A., eds., *NATO Science for Peace and Security Series B: Physics and Biophysics*, 151, Springer, Dordrecht, The Netherlands (2019). Proceedings of the NATO Advanced Research Workshop on Fundamental and Applied NanoElectroMagnetics II: THz Circuits, Materials, Devices. Minsk, Belarus, 5-7 June, 2018.
- ³³“TYDEX[®] THz band pass filters.” http://www.tydexoptics.com/products/thz_optics/thz_band_pass_filter/. Accessed: 14 August 2019.
- ³⁴“TYDEX[®] THz lenses.” http://www.tydexoptics.com/products/thz_optics/thz_lens/. Accessed: 14 August 2019.
- ³⁵Moldosanov, K. A., Postnikov, A. V., Lelevkin, V. M., and Kairyev, N. J., “Terahertz imaging technique for cancer diagnostics using frequency conversion by gold nano-objects,” *Ferroelectrics* **509**(1), 158 (2017).
- ³⁶Gallerano, G. P. and Biedron, S., “Overview of terahertz radiation sources,” in [*Proceedings of the 2004 FEL Conference*], 216 (2004).
- ³⁷Tonouchi, M., “Cutting-edge terahertz technology,” *Nature Photonics* **1**, 97 (Feb 2007).
- ³⁸Booske, J. H., “Plasma physics and related challenges of millimeter-wave-to-terahertz and high power microwave generation,” *Physics of Plasmas* **15**, 055502 (May 2008).
- ³⁹Armstrong, C. M., “The truth about terahertz.” <https://spectrum.ieee.org/aerospace/military/the-truth-about-terahertz> (2012). IEEE Spectrum (20 Aug 2012), accessed: 13 August 2019.
- ⁴⁰Kang, S., Vora, K., and Mazur, E., “One-step direct-laser metal writing of sub-100 nm 3D silver nanostructures in a gelatin matrix,” *Nanotechnology* **26**, 121001 (Mar 2015).
- ⁴¹Huo, Z., Tsung, C.-k., Huang, W., Zhang, X., and Yang, P., “Sub-two nanometer single crystal Au nanowires,” *Nano Letters* **8**, 2041 (Jul 2008). PMID: 18537294.
- ⁴²Kang, Y., Ye, X., and Murray, C. B., “Size- and shape-selective synthesis of metal nanocrystals and nanowires using CO as a reducing agent,” *Angewandte Chemie International Edition* **49**, 6156 (Aug 2010).
- ⁴³Kim, F., Sohn, K., Wu, J., and Huang, J., “Chemical synthesis of gold nanowires in acidic solutions,” *Journal of the American Chemical Society* **130**, 14442 (Nov 2008). PMID: 18850710.
- ⁴⁴Pazos-Pérez, N., Baranov, D., Irsen, S., Hilgendorff, M., Liz-Marzán, L. M., and Giersig, M., “Synthesis of flexible, ultrathin gold nanowires in organic media,” *Langmuir* **24**, 9855 (Sep 2008).
- ⁴⁵Wang, F., Dai, Y., and Zhao, J., “The fracture stabilities of ultrathin gold nanowires,” *Superlattices and Microstructures* **100**, 237 (Dec 2016).